



Development and experimental evaluation of an innovative self-boosting energy recovery device for small-scale SWRO system

Junjie Tian^{a,b,c}, Yue Wang^{a,b,c,*}, Jie Zhou^{a,b,c}, Zhisong He^{a,b,c}, Shichang Xu^{a,c,*}

^aChemical Engineering Research Center, School of Chemical Engineering and Technology, Tianjin University, Tianjin 300072, China, Tel. +86 22 85356553; emails: tdwy75@tju.edu.cn (Y. Wang), xushichang@sina.com (S. Xu), tjjie123@163.com (J. Tian), tjzhoujie@163.com (J. Zhou), hezhisongq@163.com (Z. He)

^bState Key Laboratory of Chemical Engineering, Tianjin 300072, China

^cTianjin Key Laboratory of Membrane Science and Desalination Technology, Tianjin 300072, China

Received 18 March 2019; Accepted 15 November 2019

ABSTRACT

The integrated energy recovery device (ERD) is an appropriate choice to reduce the energy consumption of the small-scale seawater reverse osmosis (SWRO) system. However, in the piston-type ERD field, the existing devices are unsuitable for application in the small-scale SWRO system. This paper introduces a self-boosting energy recovery device (SB-ERD) that employed the differential pressure chamber structure in the piston-type ERD to function as an integrated ERD, thus resolving the above application problem of piston-type ERDs. The performance of this device was experimentally evaluated using an SWRO desalination platform. The results showed that the SB-ERD could run stably with a leakage ratio of 0.55%–0.95% and an energy recovery efficiency of 91.55%–92.41% under an operating pressure of 3.0–6.0 MPa. Under the applicable optimal conditions (a feed pressure of 4.5 MPa and a recovery ratio of 17.20%), the specific energy consumption of the SWRO system coupled with the SB-ERD was 2.61 kWh/m³, which was lower than that of the SWRO system with the integrated ERD in the literature. This research indicates that the SB-ERD can achieve excellent device performance and energy conservation effect in the SWRO experimental platform, showing that the newly developed piston-type ERD possesses a good application prospect in the small-scale SWRO system.

Keywords: SWRO; Energy recovery device; Leakage; Energy recovery efficiency; Specific energy consumption

1. Introduction

Freshwater scarcity is an increasingly severe global problem because of many factors, for example, climate change and rapid population growth [1,2]. Considering the abundant seawater resources on Earth, seawater desalination can be an approach to alleviate the water crisis [3]. Seawater reverse osmosis (SWRO) technology adopts the applied pressure to overcome osmotic pressure and separate the seawater flow into two streams, that is, the permeate flow and the brine flow. Energy recovery devices (ERDs) can

recover the pressure energy of high-pressure (HP) brine discharged from the reverse osmosis (RO) membrane to reduce the energy consumption of the SWRO system [4,5]. Owing to the advantage of low energy consumption, SWRO technology is currently one of the mainstream methods in the seawater desalination market worldwide [6].

In seawater-rich sites such as sea islands and ships, a small-scale SWRO system (product water capacity per unit: 0.7–220 m³/d) can satisfy the freshwater demand [7]. In the conventional small SWRO system, ERDs are not generally used [8,9] due to either insufficient space or high equipment

* Corresponding authors.

costs. To reduce the space requirement and the equipment costs, many studies have been conducted on integrated ERDs, which integrate the functions of the isobaric ERD and the booster pump as a whole. Various integrated ERDs with a novel structural design (e.g., the iSave ERD and the Clark pump) have been developed in recent years [10–12]. The SWRO system coupled with integrated ERDs achieved low specific energy consumption (SEC) values [13,14], illustrating that the integrated ERD is an appropriate choice for the small-scale SWRO system to reduce energy consumption.

The piston-type ERD has been a popular research topic due to the advantages of low leakage and high efficiency [15,16]. In previous work by our research group, various piston-type ERDs were developed and evaluated in our laboratory. Table 1 presents a comparison of the main characteristics of these ERDs and some commercial ERDs [17–24]. However, the piston-type ERDs mentioned above all adopted the isobaric chamber structure design and were unsuitable for application in the small-scale SWRO system. Hence, finding an appropriate method to develop a piston-type ERD that performs the functions of the integrated ERD has become a key research subject in the piston-type ERD field.

This paper introduces a self-boosting energy recovery device (SB-ERD) which employed the differential pressure chamber structure in the piston-type ERD to realize the application in the small-scale SWRO system. The performance of the SB-ERD was evaluated in an SWRO experimental platform in terms of the flow and pressure characteristics of HP fluid, pressure boosting ratio, leakage, pressurizing efficiency and energy recovery efficiency. On this basis, the SEC of the SWRO system coupled with SB-ERD under the optimal operating conditions was determined and assessed by the comparison with the reported data in the open literature.

2. SB-ERD and the experimental platform

2.1. Working principle of the SB-ERD

Fig. 1 shows a structural diagram of the SB-ERD, which includes a reciprocating switcher, two hydraulic cylinders and a check valve nest. In the working position, the reciprocating switcher establishes the HP channel, through which the HP brine flows into one hydraulic cylinder, and the low-pressure (LP) channel, through which the LP brine exits from the other hydraulic cylinder. The hydraulic cylinders are the core components where the pressure exchange

between the seawater and the brine occurs, and the check valve nest is a passive component that establishes the seawater channels for performing the pressurizing and depressurizing processes in the cylinders.

2.1.1. Hydraulic cylinder of the SB-ERD

Differential pressure chamber structure has long been applied in hydraulic intensifiers and can transform a lower-pressure liquid into a higher-pressure liquid by reducing the hydraulic volume [25]. In the design process of the SB-ERD, this research employed the differential pressure chamber structure in the hydraulic cylinders of the piston-type ERD. Fig. 2 shows the differential pressure cylinders of the SB-ERD. Each hydraulic cylinder is divided into a brine chamber and a seawater chamber by the piston. The piston rod contained in the seawater chamber creates the sectional area difference between the brine chamber and the seawater chamber. The pressure energy of the HP brine is transferred to HP seawater in one cylinder, as shown in Fig. 2a and the LP brine is discharged by the LP seawater in the other cylinder, as shown in Fig. 2b. The pressurizing efficiency is introduced as the ratio of the pressure energy of the HP seawater to that of the HP brine, as shown in Eq. (1):

$$\eta_p = \frac{P_{so} \times Q_{so}}{P_{bi} \times Q_{bi}} \quad (1)$$

where P_{so} , P_{bi} , Q_{so} , and Q_{bi} are the HP seawater pressure, the HP brine pressure, the HP seawater flow rate and the HP brine flow rate, respectively.

Under ideal conditions, the pressure energy loss value is assumed to be zero ($\eta_p = 100\%$), and the mathematical design formula of the hydraulic cylinder is obtained as shown in Eq. (2), which indicates that the HP seawater pressure can be boosted higher than the HP brine pressure due to the aforementioned sectional area difference.

$$\frac{P_{so,i}}{P_{bi,i}} = \frac{Q_{bi,i}}{Q_{so,i}} = m \quad (2)$$

where the subscript i represents the ideal conditions, and m is the sectional area ratio between the brine chamber and the seawater chamber.

Table 1
Comparison of piston-type ERD characteristics

ERD name	DWEER	SalTec DT	FS-ERD	RS-ERD
Hydraulic cylinder type	Isobaric	Isobaric	Isobaric	Isobaric
Switcher type	LinX valve	Rotating valve	Rotary fluid switcher	Reciprocating switcher
Motion mode in the switching process	Reciprocating motion	Rotary motion	Rotary motion	Reciprocating motion
Driving mode of the switcher	Hydraulically or electrically driven	Motor driven	Motor driven	Hydraulically driven
Reference	[17,18]	[19,20]	[21,22]	[23,24]

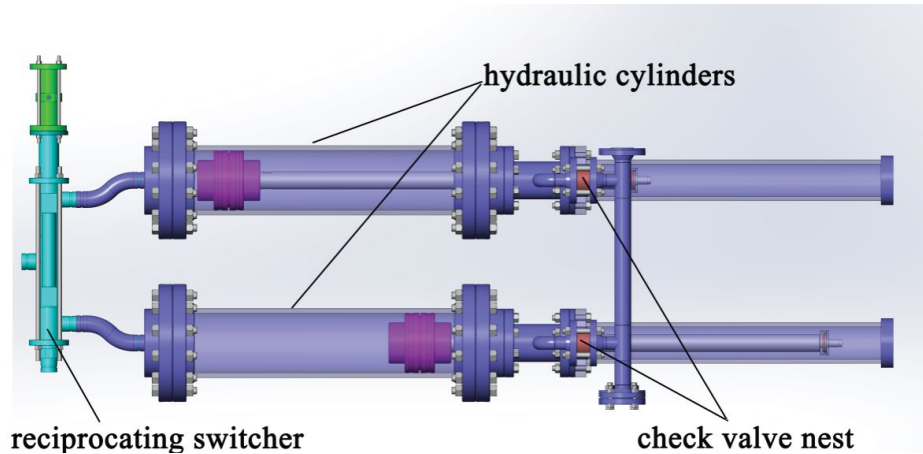


Fig. 1. Structure of the SB-ERD.

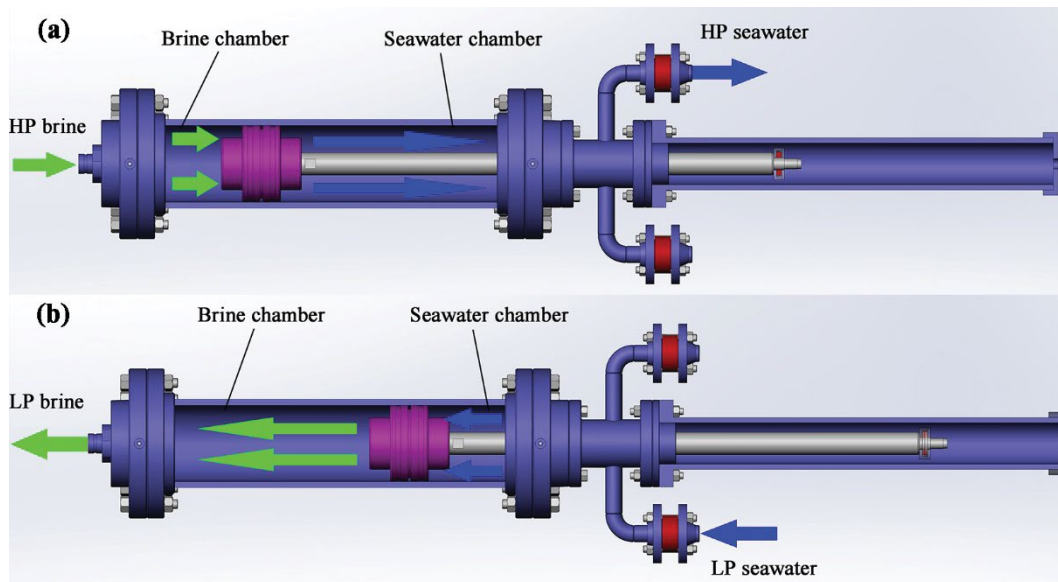


Fig. 2. Differential pressure cylinders of the SB-ERD.

However, the HP seawater pressure would not exceed the HP pump pressure. It is because that the HP pump was the hydraulic power source of HP brine which could drive the pistons in the SB-ERD to move and the outlet pressure of the HP pump was the highest pressure in the whole SWRO system. Through the above analysis, the SB-ERD could adopt the differential pressure structure to integrate the functions of the booster pump and the isobaric ERD to boost the HP seawater pressure directly to the outlet pressure level of the HP pump.

2.1.2. Structure of the reciprocating switcher

Fig. 3 presents a schematic diagram of the reciprocating switcher. The connecting ports of the switcher include two-LP brine ports, one HP brine port and two hydraulic cylinder ports, as shown in Fig. 3a (the top view). The sealing pair in the switcher is composed of the valve plate and

the corresponding valve seat. In the design, two circulating pipes are placed outside the switcher, as shown in Fig. 3b (the front view), to establish pressure difference on both sides of the valve plate that can provide the sealing force for the sealing pair. Hence, the sealing pair can adopt the self-impacted sealing principle to prevent leakage from the HP brine to the LP brine.

To save capital costs, maintenance costs and operating costs, a portion of HP brine is utilized to drive the piston to move in the actuator. Under the driving force of the hydraulic actuator, the switcher can switch between the forward position and the backward position periodically. When the switcher is in the forward position, as shown in Fig. 3c (the sectional view), the LP plate 1 and HP plate 1 are closed, while the LP plate 2 and HP plate 2 are open. Under this condition, the HP brine port and the hydraulic cylinder port 1 communicate to establish the HP channel, and the LP brine port 2 and the hydraulic cylinder port 2 communicate

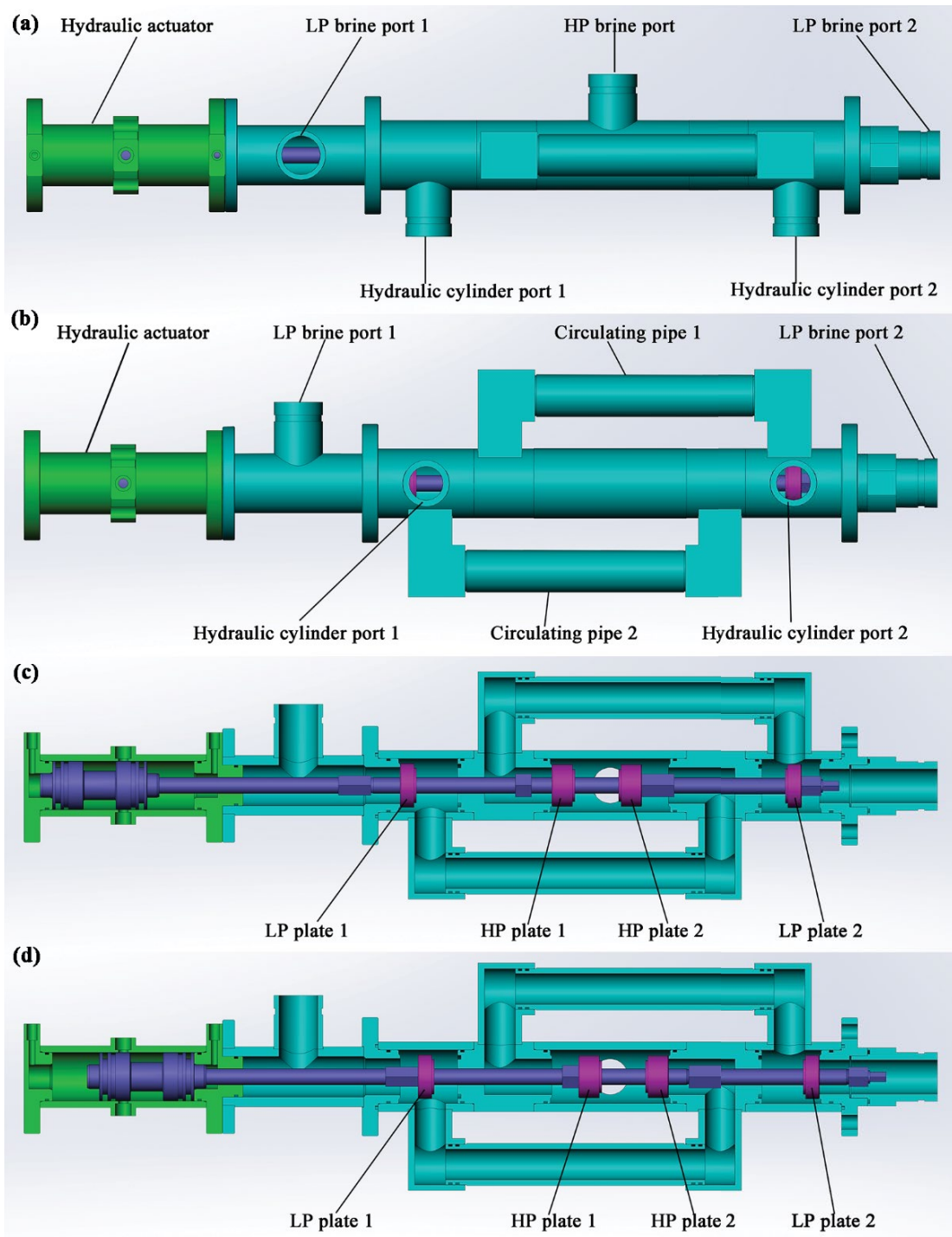


Fig. 3. Schematic diagram of the reciprocating switcher.

to establish the LP channel. When the switcher is in the backward position as shown in Fig. 3d (the sectional view), LP plate 1 and HP plate 1 are open while LP plate 2 and HP plate 2 are closed. Under this condition, the HP brine port and the hydraulic cylinder port 2 communicate to establish the HP channel, and the LP brine port 1 and the hydraulic cylinder port 1 communicate to establish the LP channel. When the switcher is in the switching process, the

HP channel overlapping function prevents overpressure on the HP brine pipeline caused by fully closing the HP channel.

2.2. Specifications of the apparatus and experimental platform

In this paper, the experiments were conducted using an SB-ERD developed in our laboratory. Detailed specifications

of the SB-ERD are listed in Table 2. The device was manufactured primarily with 316L stainless steel to prevent seawater corrosion. The piston was made with polytetrafluoroethylene (PTFE) to reduce its weight and decrease the impact force with the cylinders.

An SWRO system was established as the experimental platform to evaluate the performance of the SB-ERD. Fig. 4 is a photo of the SB-ERD in the SWRO experimental platform and Fig. 5 presents a simplified flow diagram of the SWRO system coupled with the SB-ERD. The seawater in the tank pumped by the low-pressure pump (LPP) (CNP, CHLF20-40LSWLC) was divided into two paths: the high-pressure pump (HPP) path and the SB-ERD path. The HPP (DANFOSS, Headquarters in Nordborg, Denmark, APP7.2) boosted the seawater pressure and pumped the HP seawater into the RO membrane. The HP brine discharged from the RO membrane entered the SB-ERD, participating in the pressure exchange with the LP seawater. The HP seawater from the SB-ERD joined the seawater supplied by the HPP and flowed into the RO membrane. The LP brine and permeate water flowed back into the tank to maintain the salinity of the seawater. Pressure and flow transmitters were installed in the main pipelines to measure and collect real-time data. The precision of the pressure transmitters reached $\pm 0.1\%$ and the precision of flow transmitters reached $\pm 0.5\%$, ensuring the measurement accuracy. An electric energy meter (DELIXI, headquarters in Wenzhou, China, DT862) was used to measure the electric energy consumption of the SWRO system.

The feed water was prepared using tap water and sea salt to obtain a total dissolved solids of 32,000 mg/L. The RO membrane was the core component in the seawater desalination process. The SWRO system (single-stage) was configured with three pressure vessels in parallel and two RO membrane elements in each pressure vessel. The technical



Fig. 4. A photo of the SB-ERD in the SWRO experimental platform.

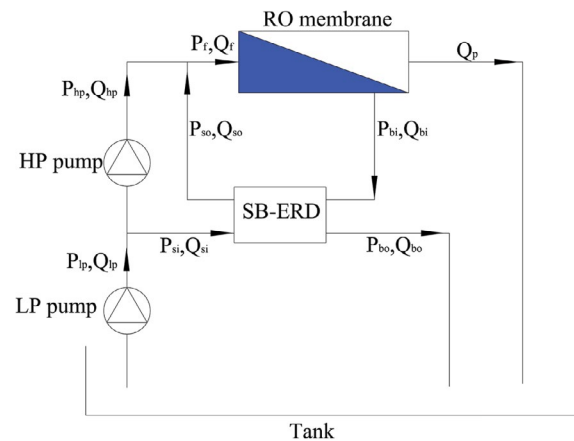


Fig. 5. Simplified flow diagram of an SWRO system coupled with an SB-ERD.

Table 2
Specifications of the SB-ERD

Parameter	Characteristic value
Reciprocating switcher	
Material	316L SS
Maximum working pressure (MPa)	6.5
Flow range (m ³ /h)	10–25
Hydraulic cylinder	
Cylinder material	316L SS
Maximum working pressure (MPa)	6.5
Flow range (m ³ /h)	10–25
<i>m</i> -value	1.055
Piston material	PTFE
Piston sealing elements	Glyd ring, guiding ring
Piston rod material	316L SS
Piston-rod sealing elements	Step seal, guiding ring, scraper seal
Check valve nest	
Material	316L SS
Maximum working pressure (MPa)	6.4
Port size (mm)	DN50

specifications of the SWRO system in our experiment are listed in Table 3.

3. Key parameters of the SB-ERD and SWRO system

3.1. Internal leakage and leakage ratio

The internal leakage is the portion of HP brine that flows into the LP brine without participating in the pressure exchange in the hydraulic cylinders. According to the definition, this value can be calculated using Eq. (3):

$$Q_1 = Q_{bi} - Q'_{bi} \quad (3)$$

where Q'_{bi} is the actual flow rate of the HP brine participating in the pressure exchange in the cylinders.

Due to the sealing elements that prevent leakage across the piston, Q'_{bi} can be calculated using Eq. (4):

$$Q'_{bi} = mQ_{so} \quad (4)$$

Hence, the calculation formula for internal leakage is obtained in Eq. (5):

Table 3
Specifications of the SWRO system

Membrane element type	Spiral-wound membrane
Membrane element model	SWC5-8040
Membrane element manufacturer	Hydranautics
Maximum operating pressure (MPa)	8.27
Maximum operating temperature (°C)	45
Maximum feed flow rate (m ³ /h)	17.0
Maximum single element recovery (%)	18
Standard water flux* (L/m ² h)	33.9
Number of pressure vessels in parallel	3
Number of elements per pressure vessel	2

*Standard water flux based on the following test conditions: 32,000 ppm NaCl solution, operating pressure of 5.5 MPa, operating temperature of 25°C, recovery ratio of 10% and pH of 6.5–7.0.

$$Q_1 = Q_{bi} - mQ_{so} \quad (5)$$

The leakage ratio can be calculated using Eq. (6):

$$\beta = \frac{Q_1}{Q_{bi}} \quad (6)$$

For the piston-type ERD, leakage mainly occurs inside the switcher. When the operating conditions (i.e., operating pressure and processing capacity) remain constant, the internal leakage and leakage ratio reflect the sealing effect inside the switcher.

3.2. Pressure boosting value and pressure boosting ratio

For the SB-ERD, the HP seawater pressure should be boosted to a value greater than the HP brine pressure such that the booster pump can be removed in the SWRO system. The pressure difference between the HP seawater and the HP brine reflects the pressurizing degree, which is defined as the pressure boosting value and can be calculated using Eq. (7).

$$\Delta P = P_{so} - P_{bi} \quad (7)$$

The pressure boosting ratio is introduced to reflect the actual pressurizing effect of the SB-ERD and is defined as the ratio of the pressure boosting value to the HP brine pressure, as shown in Eq. (8):

$$\alpha = \frac{\Delta P}{P_{bi}} \quad (8)$$

According to Eq. (2), the ideal pressure boosting ratio is equal to m^{-1} , and the actual pressure boosting ratio ranges from 0 to m^{-1} .

3.3. Energy recovery efficiency

The commonly accepted formula for energy recovery efficiency is shown in Eq. (9). The energy recovery efficiency

reflects the comprehensive performance of the SB-ERD by considering the four streams of fluids participating in the pressure exchange:

$$\eta = \frac{P_{so} \times Q_{so} + P_{bo} \times Q_{bo}}{P_{si} \times Q_{si} + P_{bi} \times Q_{bi}} \quad (9)$$

where P_{si} , P_{bo} , Q_{si} , and Q_{bo} are the LP seawater pressure, the LP brine pressure, the LP seawater flow rate and the LP brine flow rate, respectively.

3.4. Recovery ratio, salt rejection and SEC

The recovery ratio and salt rejection are two key parameters of the SWRO system that can reflect the separation performance of the RO membrane. The definition formulas of the recovery ratio and the salt rejection are expressed as Eqs. (10) and (11):

$$R_p = \frac{Q_p}{Q_f} \quad (10)$$

where Q_p and Q_f are the permeate flow rate and the feed flow rate of the RO membrane, respectively;

$$R = \frac{C_f - C_p}{C_f} \quad (11)$$

where C_f and C_p are the salt concentrations of the feed flow and the permeate flow, respectively.

According to the reported literature, the recovery ratio for the small-scale SWRO system (single-stage) commonly falls in the range of 10%–25% [9]. In our experiment, the maximum recovery ratio of the SWRO system has exceeded the above values. Hence, the recovery ratio can be adjusted to any value in the above range theoretically.

The SEC is another important parameter of the SWRO system, which has an impact on the economic cost of permeation. The SEC of permeation in the SWRO is defined as in Eq. (12):

$$SEC = \frac{W_{total}}{Q_p} = \frac{W_{hp} + W_{lp}}{Q_p} \quad (12)$$

where W_{total} is the total system power, and W_{hp} and W_{lp} are the power of the HPP and the LPP, respectively.

The power of the HPP and the LPP can be calculated by Eqs. (13) and (14):

$$Q_{hp} = \frac{\rho g Q_{hp} H_{hp}}{\eta_{m1} \eta_{p1} \eta_{VFD1}} \quad (13)$$

$$W_{lp} = \frac{\rho g Q_{lp} H_{lp}}{\eta_{m2} \eta_{p2} \eta_{VFD2}} \quad (14)$$

where Q_{hp} and Q_{lp} are the pump flow rate of the HPP and the LPP, m³/s, respectively; H_{hp} and H_{lp} are the pump head values of the HPP and the LPP, m, respectively; η_{m1} , η_{p1} , and η_{VFD1}

are the motor efficiency, pump efficiency and the variable frequency drive (VFD) efficiency of the HPP, respectively; η_{m2} , η_{p2} and η_{VFD2} are the motor efficiency, pump efficiency and the VFD efficiency of the LPP, respectively.

Using Eqs. (6), (10) and (12)–(14), the SEC of the SWRO system coupled with the SB-ERD can be expressed as follows:

$$\text{SEC} = 0.2875 \frac{(P_f - P_{ip}) [\beta(1 - R_p) + (R_p + m - 1)]}{\eta_{m1} \eta_{p1} \eta_{VFD1} R_p m} + 0.2875 \frac{P_{ip}}{\eta_{m2} \eta_{p2} \eta_{VFD2} R_p} \quad (15)$$

4. Results and discussion

In this section, the SB-ERD was evaluated in the above SWRO experimental platform. To obtain steady and reliable data, the experiment under each condition was conducted over a long period (3–4 h).

4.1. Flow and pressure characteristics of HP fluid

Because flow and pressure fluctuations have a significant impact on the running stability of the SB-ERD and the SWRO system, the flow and pressure characteristics of HP fluid should be investigated in the SWRO system. In this section, the SB-ERD was evaluated with regard to the flow and pressure characteristics of HP fluid under an operating pressure (HP brine pressure) of 6.0 MPa and a processing capacity (HP brine flow rate) of 22 m³/h.

4.1.1. Flow characteristics of HP fluid

Fig. 6 presents the flow curves of HP seawater and HP brine. The figure shows the data for only 1 min to illustrate the flow characteristics more clearly. The fluctuations in the flow curves of the HP fluid appeared periodically and maintained good time consistency with each other.

For the SB-ERD, a portion of the HP brine was utilized to drive the piston to move in the switching process of the reciprocating switcher, which could cause the flow fluctuations on the HP brine. Since that the SB-ERD followed the positive displacement principle, both the flow rate of HP brine and that of HP seawater were determined by the moving speed of the isolation piston. Hence, the fluctuations in the flow curves could keep good time consistency.

It can be noted from Fig. 6 that the flow fluctuation amplitudes of HP seawater and HP brine were 1.22 and 1.24 m³/h, respectively. Despite the existence of flow fluctuations, nearly equal flow fluctuation amplitudes were conducive to the stability of the permeate flow rate according to the mass balance of the RO membrane.

4.1.2. Pressure characteristics of HP fluid

Fig. 7 presents the pressure curves of HP seawater and HP brine. The pressure curves displayed periodical fluctuations and the pressure fluctuations of HP seawater and HP brine appeared synchronously. The similar pressure fluctuation trend of HP fluid was attributed to the unique HP

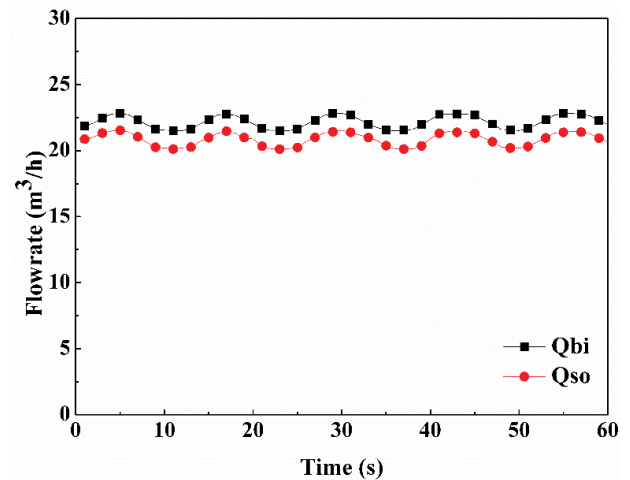


Fig. 6. Flow curves of HP seawater and HP brine.

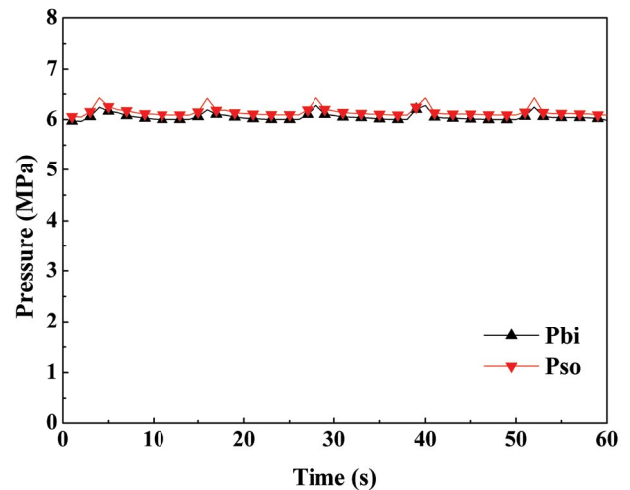


Fig. 7. Pressure curves of HP seawater and HP brine.

channel overlapping function of the reciprocating switcher, which ensured that the HP channel remained open during the switching process of the reciprocating switcher and the pressure exchange between HP seawater and HP brine in the hydraulic cylinder was carried continuously.

It can also be noted that the pressure curves of the HP fluid for the SB-ERD presented transient upward fluctuations. In the switching process of the reciprocating switcher, the pressurizing process occurred in both hydraulic cylinders simultaneously and the pistons in the hydraulic cylinders began to change the moving direction. The reversal of the piston moving direction and the inertia of the HP fluid could cause the upward pressure fluctuation of the HP fluid.

Both the pressure fluctuation amplitude of HP brine and that of HP seawater were 0.32 MPa. The small pressure fluctuations were favorable for maintaining the stability of the RO membrane inlet pressure and alleviating the damage to the RO membrane elements caused by pressure pulsation.

4.2. Device performance evaluation of the SB-ERD

4.2.1. Internal leakage and leakage ratio

Fig. 8 presents the internal leakage and leakage ratio of the SB-ERD under different operating pressures. Both the internal leakage and leakage ratio showed an increasing trend as the operating pressure increased from 3.0 to 6.0 MPa. When the operating pressure dropped to 3.0 MPa, the minimum internal leakage was 0.10 m³/h, and the corresponding leakage ratio was 0.55%. When the operating pressure increased to 6.0 MPa, the maximum internal leakage was 0.21 m³/h, and the corresponding leakage ratio was 0.95%. For the SB-ERD, the internal leakage mainly occurred across the sealing faces of the sealing pair inside the switcher when the reciprocating switcher was in the working position. The pressure difference between the HP brine and LP brine supplied the driving force for leaking, and this difference was larger under higher operating pressures. Hence, the leakage ratio increased as the operating pressure increased. Nevertheless, the sealing pressure increased with the operating pressure owing to the self-impacted sealing plates, which weakened the increasing leakage trend. Under the same operating pressure (6.0 MPa), the SB-ERD achieved a smaller leakage ratio than the data in the previous study (leakage ratio of 2.62%–3.95%) [26], which proved the superiority of the sealing structure design of SB-ERD.

4.2.2. Pressure boosting ratio

Fig. 9 gives the pressure boosting ratio of the SB-ERD under different operating pressures. It can be observed that the pressure boosting ratio presented a decreasing trend from 1.90% to 1.50% when the pressure increased, which can be explained as follows. The flow resistance loss of feed water through the RO membrane is the main part that needed to be compensated by the pressure boosting value. It was found that the feed flow rate increased moderately when the operating pressure increased from 3.0 to 6.0 MPa, which resulted in that the pressure boosting value increased slightly. Compared with the pressure boosting value, the operating pressure increased significantly. Hence, the disproportionate increases in the pressure boosting value and

the operating pressure led to a decrease in the pressure boosting ratio as the operating pressure increased.

4.2.3. Pressurizing efficiency and energy recovery efficiency

Fig. 10 presents the pressurizing efficiency and energy recovery efficiency of SB-ERD under different operating pressures. The pressurizing efficiency decreased from 96.11% to 95.31% when the operating pressure increased from 3.0 to 6.0 MPa. According to Eq. (1), the pressurizing efficiency of the SB-ERD is co-determined by the pressure boosting ratio and the leakage ratio. The increasing trend of the leakage ratio and the decreasing trend of the pressure boosting ratio led to a slight decline in the pressurizing efficiency of the SB-ERD. Nevertheless, the pressurizing efficiency could remain over 95.31% under a wide-range pressure condition, which was the basis for the high energy recovery efficiency of the SB-ERD.

From Fig. 10, the energy recovery efficiency presents a slightly increasing trend from 91.55% to 92.41% when the pressure increased from 3.0 to 6.0 MPa. The high energy

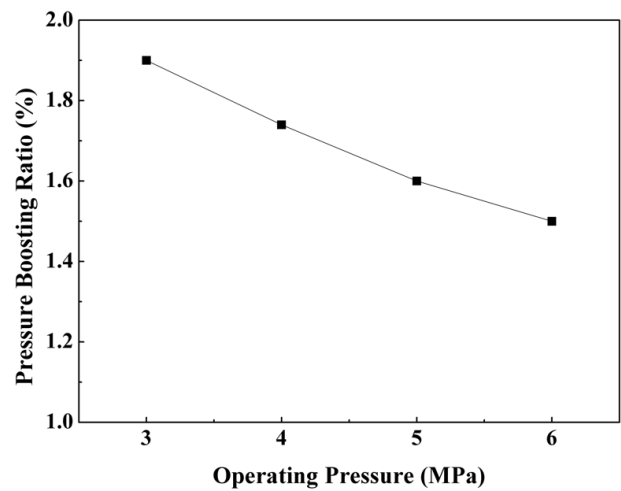


Fig. 9. Pressure boosting ratio of the SB-ERD.

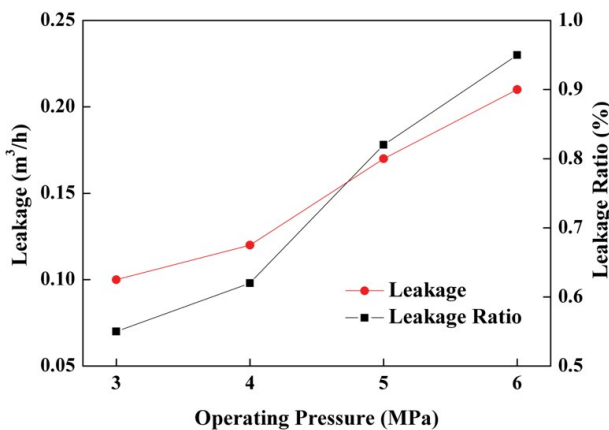


Fig. 8. Internal leakage and leakage ratio of the SB-ERD.

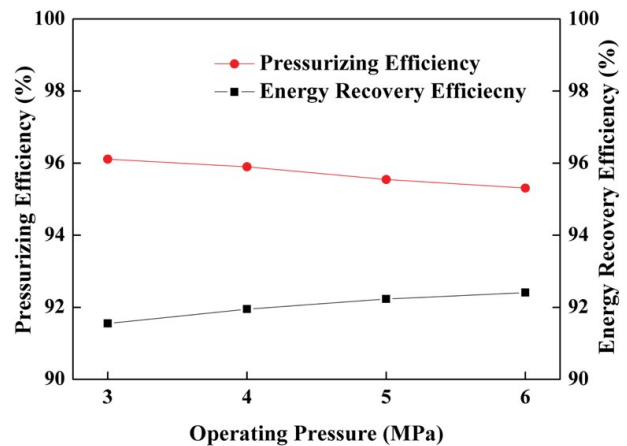


Fig. 10. Pressurizing efficiency and energy recovery efficiency of the SB-ERD.

recovery efficiency of the SB-ERD benefited from two aspects. One was the rational internal channels of the SB-ERD which decreased the flow resistance of the fluid. The other aspect was the self-impacted sealing structure in the reciprocating switcher, which made the leakage ratio of SB-ERD keep at a low level. Under the operating pressure of 6.0 MPa, the energy recovery efficiency of the SB-ERD could maintain at a high level, which is comparable to that of Clark pump (average efficiency of 93%) and iSave (93%) reported in the literature [12,27].

4.3. Energy consumption of the SWRO system coupled with the SB-ERD

In this section, the energy consumption of the SWRO system coupled with the SB-ERD was evaluated by the experimental pathway. According to Eq. (15), the SEC of the SWRO system decreased as the recovery ratio increased and the other parameters remained constant. It can also be noted that the SEC of the SWRO system increased linearly with the feed pressure if the other parameters were invariable. According to the change trends of the SEC vs. the feed pressure and the recovery ratio, the better SEC value can be obtained under the lower feed pressure and the higher recovery ratio.

However, the above theoretical analysis did not consider the restrictions of the operating conditions. The experiments were conducted to obtain the optimal SEC under applicable operating conditions.

In the experiments, it was found that the recovery ratio cannot be adjusted independently from the feed pressure due to the absence of the booster pump. Fig. 11 gives the experimental recovery ratio, salt rejection and SEC data under different feed pressures using the SB-ERD in the SWRO system. In the feed pressure range of 4.0–6.0 MPa, the recovery ratio increased from 16.60% to 18.05% and the SEC presented an increasing trend from 2.41 to 3.30 kWh/m³. Due to the slight increase of the recovery ratio, the feed pressure became the factor affecting the SEC more significantly than the recovery ratio. From Fig. 11, the salt rejection increased from 98.99% to 99.56% in the above pressure range, which illustrated that the desalting effect worsened under the lower pressure condition. Hence, the salt rejection of the RO membrane should be considered in the selection of the optimal operating point. The electrical conductivity of typical drinking water is below 500 $\mu\text{S}/\text{cm}$ [28,29]. The corresponding salt rejection should be above 99.22% according to calculating using Eq. (11). Considering the goals of minimizing the SEC and meeting the drinking water demand, the optimal operating point was found under the conditions of a feed pressure of 4.5 MPa and a recovery ratio of 17.20%. Under the above optimal conditions, the SEC of the SWRO system coupled with the SB-ERD was 2.61 kWh/m³. In the open literature, the SEC of the SWRO system coupled with the integrated ERD (Clark pump) was 3.76–3.90 kWh/m³ under lower feed pressure (3.81–3.87 MPa) and similar recovery ratio (17%–19%) [30]. According to the above comparison, the SEC of the SWRO system with the SB-ERD was relatively low, indicating that the SB-ERD played an important role in reducing the energy consumption of the SWRO system.

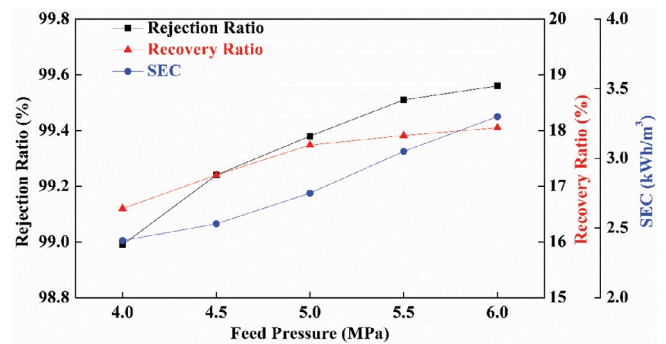


Fig. 11. Experimental recovery ratio, salt rejection and SEC data under different feed pressures.

5. Conclusions

An SB-ERD employing the differential pressure chamber structure in the piston-type ERD was developed and evaluated in an SWRO experimental platform. The conclusions can be obtained from the experimental results as follows.

First, the SB-ERD could boost the pressure of the LP seawater stream to the inlet pressure level of the RO membrane under different operating conditions, illustrating that this integrated ERD possesses the function of the booster pump and can be applied in the small-scale SWRO system.

Second, the SB-ERD could run stably with a small leakage ratio of 0.55%–0.95% and a high energy recovery efficiency of 91.55%–92.41% in the operating pressure range of 3.0–6.0 MPa, proving the superiority of the sealing structure and the device performance.

Third, the energy consumption of the SWRO system coupled with the SB-ERD was studied through the experimental pathway. Under the optimal conditions (a feed pressure of 4.5 MPa and a recovery ratio of 17.20%), the SWRO system coupled with the SB-ERD achieved an SEC of 2.61 kWh/m³, which was lower than the SEC of the SWRO system with the integrated ERD in the literature.

Symbols

C_f	—	Salt concentration of the feed flow
C_p	—	Salt concentration of the permeate flow
m	—	Sectional area ratio between the brine chamber and the seawater chamber
H_{hp}	—	Pump head of the HPP
H_{lp}	—	Pump head of the LPP
P_{so}	—	HP seawater pressure
P_{si}	—	LP seawater pressure
P_{bo}	—	LP brine pressure
P_{bi}	—	HP brine pressure
$P_{bi,i}$	—	Ideal HP brine pressure
$P_{so,i}$	—	Ideal HP seawater pressure
P_f	—	Feed pressure of the reverse osmosis membrane
P_{hp}	—	Outlet pressure of the HPP
P_{lp}	—	Outlet pressure of the LPP
Q_{so}	—	HP seawater flow rate
Q_{si}	—	LP seawater flow rate
Q_{bo}	—	LP brine flow rate
Q_{bi}	—	HP brine flow rate

$Q_{bi,i}$	—	Ideal HP brine flow rate
$Q_{so,i}$	—	Ideal HP seawater flow rate
Q_l	—	Internal leakage of the ERD
Q'_{bi}	—	Actual HP brine flow rate participating in the pressure exchange in the cylinders
Q_f	—	Feed flow rate of the reverse osmosis membrane
Q_{hp}	—	HPP flow rate
Q_{lp}	—	LPP flow rate
Q_p	—	Permeate flow rate
R	—	Salt rejection
R_p	—	Recovery ratio
W_{hp}	—	Power of the HPP
W_{lp}	—	Power of the LPP
W_{total}	—	Total system power
ΔP	—	Pressure boosting value
α	—	Pressure boosting ratio
β	—	Leakage ratio of the ERD
η	—	Energy recovery efficiency
η_p	—	Pressurizing efficiency
η_{m1}	—	Motor efficiency of the HPP
η_{p1}	—	Pump efficiency of the HPP
η_{VFD1}	—	VFD efficiency of the HPP
η_{m2}	—	Motor efficiency of the LPP
η_{p2}	—	Pump efficiency of the LPP
η_{VFD2}	—	VFD efficiency of the LPP

Acknowledgment

This study is supported by National Key R&D Program of China (2017YFC0403800).

References

[1] J. Schewe, J. Heinke, D. Gerten, I. Haddeland, N.W. Arnell, D.B. Clark, R. Dankers, S. Eisner, B.M. Fekete, F.J. Colon-Gonzalez, S.N. Gosling, H. Kim, X. Liu, Y. Masaki, F.T. Portmann, Y. Satoh, T. Stacke, Q. Tang, Y. Wada, D. Wisser, T. Albrecht, K. Frieler, F. Piontek, L. Wars-zawski, P. Kabat, Multimodel assessment of water scarcity under climate change, *Proc. Natl. Acad. Sci. U.S.A.*, 111 (2014) 3245–3250.

[2] H. Shemer, R. Semiat, Sustainable RO desalination - energy demand and environmental impact, *Desalination*, 424 (2017) 10–16.

[3] A.D. Khawaji, I.K. Kutubkhanah, J.M. Wie, Advances in seawater desalination technologies, *Desalination*, 221 (2008) 47–69.

[4] N. Liu, Z. Liu, Y. Li, L. Sang, Studies on leakage characteristics and efficiency of a fully-rotary valve energy recovery device by CFD simulation, *Desalination*, 415 (2017) 40–48.

[5] T.A. El-Sayed, A.A. Abdel Fatah, Performance of hydraulic turbocharger integrated with hydraulic energy management in SWRO desalination plants, *Desalination*, 379 (2016) 85–92.

[6] N. Melián-Martel, J.J. Sadhwani Alonso, S.O. Pérez Báez, Reuse and management of brine in sustainable SWRO desalination plants, *Desal. Wat. Treat.*, 51 (2013) 560–566.

[7] A.S. Stillwell, M.E. Webber, Predicting the specific energy consumption of reverse osmosis desalination, *Water*, 8 (2016) 601.

[8] E.S. Mohamed, G. Papadakis, E. Mathioulakis, V. Belessiotis, An experimental comparative study of the technical and economic performance of a small reverse osmosis desalination system equipped with an hydraulic energy recovery unit, *Desalination*, 194 (2006) 239–250.

[9] V.G. Gude, Energy consumption and recovery in reverse osmosis, *Desal. Wat. Treat.*, 36 (2011) 239–260.

[10] Danfoss, Energy Recovery Devices for Reverse Osmosis Applications, Available at: <https://www.danfoss.com/en/products/energy-recovery-devices/dcs/energy-recovery-devices-for-reverse-osmosis-applications/#/> (Accessed 18 March 2019).

[11] M. Thomson, D. Infield, Laboratory demonstration of a photovoltaic-powered seawater reverse-osmosis system without batteries, *Desalination*, 183 (2005) 105–111.

[12] M. Thomson, M.S. Miranda, D. Infield, A small-scale seawater reverse-osmosis system with excellent energy efficiency over a wide operating range, *Desalination*, 153 (2003) 229–236.

[13] V. Pikalov, S. Arrieta, A.T. Jones, J. Mamo, Demonstration of an energy recovery device well suited for modular community-based seawater desalination systems: result of Danfoss iSAVE 21 testing, *Desal. Wat. Treat.*, 51 (2013) 4694–4698.

[14] E.S. Mohamed, G. Papadakis, E. Mathioulakis, V. Belessiotis, The effect of hydraulic energy recovery in a small sea water reverse osmosis desalination system; experimental and economical evaluation, *Desalination*, 184 (2005) 241–246.

[15] B. Schneider, Selection, operation and control of a work exchanger energy recovery system based on the Singapore project, *Desalination*, 184 (2005) 197–210.

[16] M.J. Guirguis, Energy Recovery Devices in Seawater Reverse Osmosis Desalination Plants with Emphasis on Efficiency and Economical Analysis of Isobaric versus Centrifugal Devices, University of South Florida, 2011.

[17] B. Schneider, Design Enhancements, IDA World Congress/Perth Convention and Exhibition Centre (PCEC), 2011.

[18] S. Mirza, Reduction of energy consumption in process plants using nanofiltration and reverse osmosis, *Desalination*, 224 (2008) 132–142.

[19] S. Bross, W. Kochanowski, SWRO core hydraulic module – the right concept decides in terms of energy consumption and reliability Part II. Advanced pressure exchanger design, *Desalination*, 165 (2004) 351–361.

[20] S. Bross, W. Kochanowski, SWRO core hydraulic system: Extension of the SalTec DT to higher flows and lower energy consumption, *Desalination*, 203 (2007) 160–167.

[21] Z. Wang, Y. Wang, Y. Zhang, B. Qi, S. Xu, S. Wang, Pilot tests of fluid-switcher energy recovery device for seawater reverse osmosis desalination system, *Desal. Wat. Treat.*, 48 (2012) 310–314.

[22] D. Song, Y. Wang, S. Xu, Z. Wang, H. Liu, S. Wang, Control logic and strategy for emergency condition of piston type energy recovery device, *Desalination*, 348 (2014) 1–7.

[23] D. Song, Y. Wang, N. Lu, H. Liu, E. Xu, S. Xu, Development and stand tests of reciprocating-switcher energy recovery device for SWRO desalination system, *Desal. Wat. Treat.*, 54 (2015) 1519–1525.

[24] D. Song, Y. Wang, S. Xu, J. Gao, Y. Ren, S. Wang, Analysis, experiment and application of a power-saving actuator applied in the piston type energy recovery device, *Desalination*, 361 (2015) 65–71.

[25] J.J. Kolle, K. Theimer, T. Theimer, R. Cox, S.R. Scherschel, Coiled Tubing Jet Drilling with a Downhole Pressure Intensifier, SPE/ICoTA Coiled Tubing and Well Intervention Conference and Exhibition, Woodlands, Texas, USA, 2008.

[26] J. Zhou, Y. Wang, Y. Duan, J. Tian, S. Xu, Capacity flexibility evaluation of a reciprocating-switcher energy recovery device for SWRO desalination system, *Desalination*, 416 (2017) 45–53.

[27] D. Michas, Design of an Energy Recovery Concept for a Small-scale Renewable-driven Reverse Osmosis Desalination System, Delft University of Technology, 2013.

[28] Wikipedia, Purified Water, Available at: https://en.wikipedia.org/wiki/Purified_water (Accessed 18 March 2019).

[29] Wikipedia, Conductivity (Electrolytic), Available at: [https://en.wikipedia.org/wiki/Conductivity_\(electrolytic\)](https://en.wikipedia.org/wiki/Conductivity_(electrolytic)) (Accessed 18 March 2019).

[30] A.S. Bermude, An Energy Recovery Device for Small-Scale Seawater Reverse Osmosis Desalination, Loughborough University, 2010.